

# MultiView High Precision VLBI Astrometry at Low Frequencies

María J. RIOJA<sup>1,2,3</sup>, Richard DODSON<sup>1</sup>, Gabor OROSZ<sup>4</sup>, Hiroshi IMAI<sup>4,5</sup>, Sandor FREY<sup>6</sup>

<sup>1</sup> *ICRAR, M468, University of Western Australia, 35 Stirling Hwy, Perth 6009, Australia*

<sup>2</sup> *CSIRO Astronomy and Space Science, 26 Dick Perry Avenue, Kensington WA 6151, Australia*

<sup>3</sup> *OAN (IGN), Alfonso XII, 3 y 5, 28014 Madrid, Spain*

<sup>4</sup> *Graduate School of Science and Engineering, Kagoshima University, 1-21-35 Korimoto, Kagoshima 890-0065, Japan*

<sup>5</sup> *Science and Engineering Area of Research and Education Assembly, Kagoshima University, 1-21-35 Korimoto, Kagoshima 890-0065, Japan*

<sup>6</sup> *Konkoly Observatory, MTA Research Centre for Astronomy and Earth Sciences, PO Box 67, H-1525 Budapest, Hungary*

maria.rioja@icrar.org

## ABSTRACT

The arrival of the Square Kilometer Array (SKA) will revitalise all aspects of Very Long Baseline Interferometry (VLBI) astronomy at the lower frequencies. In the last decade there have been huge strides towards routinely achieving high precision VLBI astrometry at frequencies dominated by the tropospheric contributions, most notably at 22GHz, using advanced phase referencing techniques. Nevertheless to increase the capability for high precision astrometric measurements at low radio frequencies (<8 GHz) an effective calibration strategy of the systematic ionospheric propagation effects that is widely applicable is required. Observations at low frequencies are dominated by distinct direction dependent ionospheric propagation errors, which place a very tight limit on the angular separation of a suitable phase referencing calibrator.

The MultiView technique holds the key to the compensation of atmospheric spatial-structure errors, by using observations of multiple calibrators and 2-D interpolation. In this paper we present the first demonstration of the power of MultiView using three calibrators, several degrees from the target, along with a comparative study of the astrometric accuracy between MultiView and phase-referencing techniques.

MultiView calibration provides an order of magnitude improvement in astrometry with respect to conventional phase referencing, achieving  $\sim 100$  micro-arcseconds astrometry errors in a single epoch of observations, effectively reaching the thermal noise limit.

MultiView will achieve its full potential with the enhanced sensitivity and multibeam capabilities of SKA and the pathfinders, which will enable simultaneous observations of the target and calibrators. Our demonstration indicates that the 10 micro-arcseconds goal of astrometry at 1.6GHz using VLBI with SKA is feasible using the MultiView technique.

*Subject headings:* techniques: interferometric, astrometry, radio continuum, line: (individual:OH128.6-50.1, WX Psc)

## 1. Introduction

Very Long Baseline Interferometry (VLBI) observations hold the potential to achieve the highest astrometric accuracy in astronomy, provided that the fringe phase observable can be calibrated (Alef 1988). The development of advanced phase referencing (PR) techniques to compensate for the tropospheric propagation errors have led to routinely achieving micro-arcsecond ( $\mu\text{as}$ ) astrometry at frequencies between ca. 10 and a few tens of GHz using alternating observations of the target and a nearby calibrator, which can be up to a few degrees away (Reid & Brunthaler 2004; Honma et al. 2008). The increasingly fast tropospheric fluctuations at higher frequencies set an upper threshold for application of PR techniques at  $\sim 43$  GHz (with but a single case at 86 GHz (Porcas & Rioja 2002)). More recently, the development of phase calibration techniques using (nearly) simultaneous observations at multiple mm-wavelengths, that is Source Frequency Phase Referencing (SFPR) (Rioja & Dodson 2011) and Multi Frequency Phase Referencing (MFPR) (Dodson et al. 2016), have extended the capability to measure  $\mu\text{as}$  astrometry up to mm-wavelengths. This capability for accurate astrometry has resulted in a wide applicability to many scientific problems (Reid & Honma 2014, and references therein). Nevertheless the application of these advanced PR techniques to relatively low frequencies  $\leq 8$  GHz are hindered by the contribution of ionospheric propagation effects, increasingly dominant at lower frequencies, which have a different nature to the tropospheric effects. The unpredictability of the spatial irregularities in the plasma density in the ionosphere introduces differential path variations between the sky directions of the two sources, and propagate into systematic position errors even for small source separations. In addition, at the lowest frequencies, the temporal variations are also an issue. These both are responsible for degrading the positional accuracy

achieved with this technique and, eventually, prevent the phase connection process and the use of conventional phase referencing.

Therefore, a new strategy is required to overcome the limitations imposed by the ionospheric propagation medium and to reach the full potential of the instruments working on these spectral regimes, such as the Square Kilometer Array (SKA) that will have VLBI capability between 0.3 and 14 GHz. In general, observations which involve more than one calibrator have demonstrated advantages for astrometric VLBI at low frequencies (Fomalont & Kopeikin 2002; Rioja et al. 2002; Doi et al. 2006). The alternative is the unusual configuration when a target and a strong calibrator lie within the field-of-view (FoV) of the VLBI antennas (i.e. an ‘in-beam’ calibrator), and thus can be observed simultaneously (Wrobel et al. 2000; Fomalont et al. 1999). A useful variation of this combines the observations of a weak ‘in-beam’ calibrator source and nodding to a strong more distant calibrator (Doi et al. 2006). The observations of the strong calibrator are used to remove the first-order atmospheric effects; then the observations of the weak ‘in-beam’ source, which is observed along with the target source, provide further adjustments of the spatial and temporal fluctuations, with longer coherence times. The results obtained with this approach are positive, however its widespread application is still limited by sensitivity. Another useful approach is when there are two calibrators aligned with, but on opposite sides of, the target (Fomalont & Kopeikin 2002). During the observations the telescopes alternate every few minutes between the three sources, and in the analysis successive scans on the calibrators are used for the spatial and temporal interpolation to the enclosed position and scan time of the target source. The rare source configuration required for this approach to work results in limited applicability, and the calibration time overhead is large.

In this paper we present results from the MultiView technique which, by deriving 2D phase screens from observations of three or more calibrators, achieves a superior mitigation of atmospheric errors that results in increased precision astrometry, along with wide applicability by relaxing the constraints on the angular separation up to few degrees, and does not require alignment of sources. The scope of application is for the low frequency regime where the performance of PR is degraded due to the spatial structure of the ionospheric dominant errors. It is a development of the “cluster–cluster” VLBI technique, which allowed simultaneous observations of a target and multiple calibrators around it by replacing single telescopes by sites with multiple elements (Rioja et al. 1997). The ability of the “cluster–cluster” technique to address the ionospheric effects has been demonstrated with joint observations between connected interferometer arrays at 1.6 GHz of a target and three calibrator sources (Rioja et al. 2002, 2009). Despite these benefits its use has been limited by the shortage of compatible observing sites, and the complexity in its implementation.

We revisit this technique in the light of the next generation of instruments for low frequency observations that will become operational in the course of the next decade. These have the multi-beam capability as an in-built feature, such as the Australian SKA Pathfinder (ASKAP) in the near future, and SKA in the longer term. We believe that the implementation of MultiView techniques will enhance the performance of VLBI observations, by providing higher precision astrometric measurements of many targets at low frequencies.

In this paper we describe the observations in Section 2; the basis of the MultiView technique in Section 3; Section 4 presents a demonstration and quantifies its astrometric capabilities, along with a comparative study with outcomes from conventional PR techniques for a range of target–calibrator angular separations, including in-beam phase referencing, using VLBA observations at 1.6 GHz; Section 5 are discussions and conclusions.

## 2. Observations

In an effort to demonstrate the improvements by MultiView calibration over conventional techniques, we conducted two epochs of observations with the NRAO<sup>1</sup> Very Long Baseline Array (VLBA) separated by one month, on 2015 June 8 (Epoch I, obs. id: BO047A7) and July 7 (Epoch II, obs. id: BO047A4), at 1.6 GHz. Both epochs of observations used identical setups with a duration of  $\sim 4$  hours. Table 1 lists the source names and coordinates and Fig. 1 shows the distribution in the sky.

The observations consisted of alternated scans switching between all the sources with a duty cycle of  $\sim 5$  minutes. The two sources in the centre of the distribution, the OH maser source and the quasar C4, were observed simultaneously because they lie within the primary beam of the VLBA antennas. They are the targets of the analyses presented in this paper, allowing the MultiView calibration to be tested for both a maser line and quasar continuum observations simultaneously. The sessions were long enough to ensure sufficient  $(u, v)$  coverage and sensitivity, spending  $\sim 40\%$  of the time on the OH–C4 pair with alternating 30–90 s scans on the C1, C2 and C3 calibrators. Both epochs were observed at a similar time range around early morning, 12:06:00–16:06:00 UT for Epoch I and 11:12:00–15:12:00 UT for Epoch II, when the variations in the ionosphere and its effects on astrometry are expected to be the largest.

The 2-bit quantized signals were recorded in dual circular polarization with 256 Mbps

---

<sup>1</sup>The National Radio Astronomy Observatory is a facility of the National Science Foundation operated under cooperative agreement by Associated Universities, Inc.

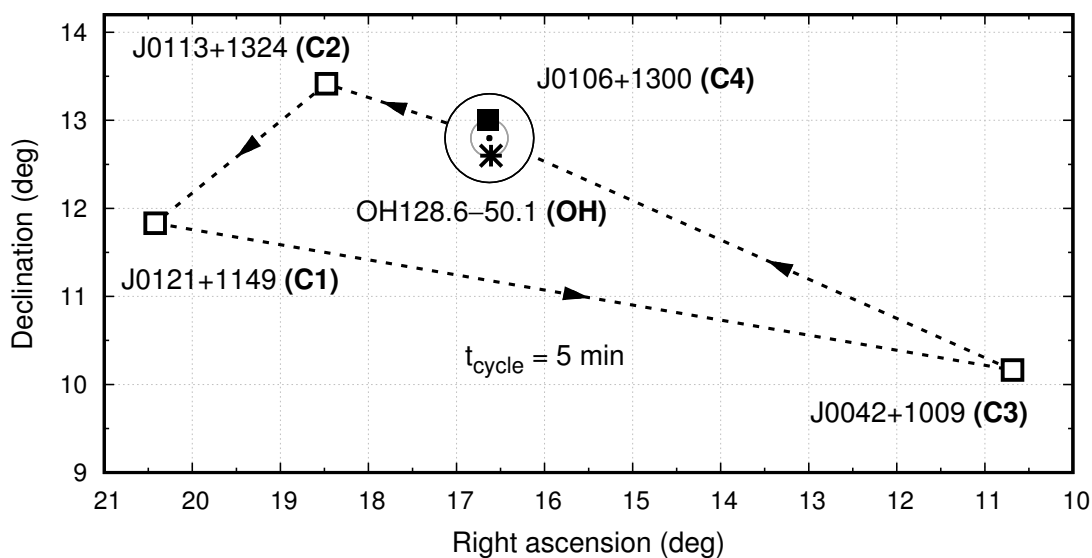


Fig. 1.— Sky distribution of the sources observed with the VLBA at 1.6 GHz. Table 1 lists the source coordinates. Dashed lines and arrows mark the source switching order during the observations with 5-min duty cycles. Star and solid symbols mark the simultaneously observed OH–C4 pair, with the VLBA antennas pointed halfway between the two. The two concentric circles represent the half-power beamwidth and full beamwidth of the antennas. Both OH and C4 are targets in the astrometric analyses (see Table 2 for description of analyses). C1 was used as the fringe-finder.

Source Name	Alias	Right Ascension ( h m s )	Declination ( ° ' " )	$\sigma_{RA}$ (mas)	$\sigma_{DEC}$ (mas)	$S_{1.6 \text{ GHz}}$ (Jy beam <sup>-1</sup> )
J0121+1149	C1	01 21 41.595044	+11 49 50.41304	0.10	0.10	2.1
J0113+1324	C2	01 13 54.510365	+13 24 52.47783	0.26	0.38	0.08
J0042+1009	C3	00 42 44.371738	+10 09 49.20750	0.15	0.17	0.17
J0106+1300	C4	01 06 33.356509	+13 00 02.60390	0.14	0.19	0.07
OH128.6–50.1	OH	01 06 25.98	+12 35 53.0			0.11

Table 1: All observed sources: four quasars and one OH-maser line source (also known as WX Psc). Columns 1 and 2 are the source names and aliases used through this paper, respectively. Columns 3 and 4 are the Right Ascension and Declination coordinates used at the correlator. Columns 5 and 6 are the corresponding position errors, if available. Column 7 is the peak brightness at 1.6 GHz measured from our observations. For quasars, all quantities are from the VLBA Radio Fundamental Catalog (L. Petrov, solution rfc\_2015b (unpublished) available on the Web at [http://asrtogeo.org/vlbi/solutions/rfc\\_2015b](http://asrtogeo.org/vlbi/solutions/rfc_2015b)). For the OH-maser, position comes from the SIMBAD Astronomical Database (<http://adsabs.harvard.edu/abs/2000A%26AS..143....9W>)

using 4 intermediate frequency (IF) bands, each with a bandwidth of 8 MHz. The IFs were spread out over 300 MHz, centered around the four ground-state OH maser lines of 1612, 1665, 1667, 1720 MHz and the HI line at 1420 MHz. Each band had a channel spacing of 1.95 kHz, corresponding to a velocity resolution of 0.36 km s<sup>-1</sup>. All bands were correlated in a single run, using two phase centers for the observations of the OH–C4 pair. For the OH maser source, only the 1612 MHz transition provided useful astrometric data.

### 3. Astrometric Data Analyses

We have carried out a comparative astrometric study using different calibration techniques and angular separations, summarized in Table 2, on the same observations. The analyses comprise conventional PR techniques using pairs of sources (i.e. one calibrator and one target source) with angular separations of  $\sim 0.4^\circ$  (i.e. in-beam),  $2^\circ$ ,  $4^\circ$  and  $6^\circ$ , and MultiView (MV) techniques using four sources (i.e. three calibrators and one target sources). The targets are the quasar C4 and the OH maser source, while the calibrators are quasars in all cases. We use the alternating quasar-only observations for the comparison between PR with a range of angular separations and MV techniques, using C4 as the target; using the OH maser source as target, we compare in-beam PR with C4 as reference,  $0.4^\circ$  away, to MV using three calibrators  $2^\circ$ ,  $4^\circ$ , and  $6^\circ$  away. Note that the MV observations in this

paper involve source switching. The repeatability of the astrometric measurements between the two epochs (i.e. inter-epoch differences) is the chosen figure of merit for our comparative study of the calibration strategies. For the quasars-only analysis, the repeatabilities are a direct indication of the uncompensated ionospheric errors remaining after calibration, given that no source position changes are expected. For the OH maser analysis, the apparent source motion due to the proper motion and parallax needs to be accounted for first, even over a 1 month timeline. Sect. 3.2 will cover the astrometric error analysis.

The PR analyses were carried out following standard procedures in the Astronomical Image Processing System (AIPS) software (Greisen 2003). The MV analyses were carried out following the same procedures in AIPS but with additional steps to incorporate direction dependent effects, as described in Section 3.1. Also, we have made self calibration maps of all sources using conventional hybrid mapping techniques in VLBI using AIPS and Difmap (Shepherd et al. 1994); these have been used to remove the source structure contribution, to provide reference points for the astrometric analysis and to assess the quality of the calibration strategies using the fractional flux recovery quantity (see Section 3.2).

### 3.1. Basis of MultiView Direction Dependent Phase Calibration

The MV calibration strategy corrects for the direction dependent nature of the ionospheric phase errors by using simultaneous or near-simultaneous observations of multiple calibrators around the target. Then we use a 2-D interpolation of the antenna phases, estimated along the directions of all calibrators, to provide corrections along the line of sight of the target observations. This is realized by a weighted linear combination of the complex antenna gains, representing the relative source distribution in the sky, as shown in Fig. 1 for the case of interest to this paper. This is equivalent to the treatment of the propagation medium as a wedge-like spatial structure, up to several degrees in size, above each antenna (Fomalont & Kopeikin 2002; Rioja et al. 2002). The temporal structure of the propagation medium effects is best calibrated using simultaneous observations of the calibrators and the target sources in MV observations. However when this observing configuration is not possible one can use alternating observations of the sources, as long as the duty cycle is less than the atmospheric coherence time.

Therefore, in MV, the target position is tied to the assumed positions of the multiple calibrators weighted as in the analysis. That is, to a virtual point in the sky whose location depends on the source distribution in the sky. Instead, in PR, the measured target positions are tied to the assumed position of the corresponding (single) calibrator. Nevertheless, as long as the calibrator sources provide good fiducial points (i.e. are stationary), this virtual

point is also stationary and changes between the astrometric measurements at different epochs trace the motion of the target in both MV and PR.

Our implementation of the MV direction dependent calibration strategy is more complicated than a basic linear interpolation. It includes a correction for untracked  $2\pi$  phase ambiguities in the measured calibrator phases, which lead to errors in the spatial interpolation. Those are automatically detected by searching over ambiguities in the formation of every interpolation and optimizing the result. Additionally we have the ability to steer the corrections by forcing the addition of ambiguities at the outset.

Astrometric Calibration	Target Source(s)	Reference Source	Angular Separation	Analysis Id.
<i>Single Calibrator</i>				
PR	C4	C2	$1.84^\circ$	PR <sub>2°</sub>
PR	C4	C1	$3.88^\circ$	PR <sub>4°</sub>
PR	C4	C3	$6.49^\circ$	PR <sub>6°</sub>
‘in beam’ PR	OH	C4	$0.4^\circ$	PR <sub>in-beam</sub>
<i>Three Calibrators</i>				
MV	C4	C1, C2, C3	$1.84^\circ, 3.88^\circ, 6.49^\circ$	MV <sub>QSO</sub>
MV	OH	C1, C2, C3	$2.0^\circ, 3.81^\circ, 6.30^\circ$	MV <sub>OH</sub>

Table 2: Astrometric analyses compared in this paper, along with aliases used throughout the text. Column 1 are the calibration techniques: using a single calibrator, regardless that the observations of the pair are carried out using source switching or simultaneously observed, and using three calibrators; PR=Phase Referencing and MV = MultiView. Columns 2 and 3 list of target and reference sources, respectively. Column 4 is the target-calibrator(s) angular separation. Column 5 is the analysis identification name used throughout the text. All analyses have been carried out for epochs I and II, separated by one month.

Target Source	Weight <sub>1</sub>	Weight <sub>2</sub>
J0106+1300 (C4)	1.147	0.1735
OH128.6-50.1 (OH)	0.985	0.2475

Table 3: MultiView weights used to implement the direction dependent ionospheric calibration along the line of the sight of the target source in the analyses. Column 1 lists the target sources, for analyses MV<sub>QSO</sub> and MV<sub>OH</sub>, respectively. Columns 2 and 3 are the weights that were applied for the phase transfer between C2 and C1 (“Weight<sub>1</sub>”), and between C3 and this combination (“Weight<sub>2</sub>”), for the calibration of the corresponding target source.



### 3.2. Error Analysis

We describe here the approaches used to quantify the uncertainties of the astrometric measurements in this paper.

1) *Repeatability errors*: We have used the repeatability of the measured positions between the two epochs of observations, which provide independent measurements of the relative source position, as an empirical estimate of the astrometric errors. The span ( $\Delta_{I-II}$ ) of the positions are indicative of uncompensated systematic ionospheric residual errors remaining after calibration for each analysis. The repeatability errors, corrected for the bias introduced by having only two measurements, are calculated as:  $\sigma_{pos,rep} = \Delta_{I-II}/\sqrt{2} * \sqrt{2/\pi}$ . They are a measure of the precision of the calibration method, in absence of inherent position changes, and we use them as the figure of merit for the comparative study. Note that while there is a limited sample of two epochs the different analyses are carried out on the same observations, enabling a direct comparison of the compensation efficiency of the systematic errors under the same weather conditions.

2) *Thermal noise (and other random) errors*: The ratio of the synthesized beam size ( $\theta_B$ ) and the signal-to-noise ratio (SNR) in the astrometric maps (i.e. PRed and MVED maps) gives an estimate of the uncertainty in the measurement of the position of a feature in the maps due to random noise, as  $\sigma_{pos,thermal} \sim 0.5\theta_B/SNR$ . This error has a contribution from thermal (usually dominated by the receiver) random noise, and from residual atmospheric phase fluctuations. The latter depends on the duty cycle during the observations, the angular separation between sources and the weather conditions. It is commonly referred to as the thermal noise error and represents the ultimate astrometric precision achievable, in absence of any other error contributions. It is usually overwhelmed by other systematic contributions.

3) *Fractional Flux Recovery*: The fractional flux recovery (FFR) quantity is defined as the ratio between the peak brightness in the astrometric maps (i.e. PRed and MVED maps) and the self-calibrated maps of the same source. It is a useful quantity for comparison between methods and is related to the thermal noise error. It provides an empirical estimate of the residual uncorrelated errors, such as atmospheric phase fluctuations, which result in image coherence losses. In general, image coherence losses arise from residual short term phase fluctuations, hence it is expected to increase with larger duty cycles (in our case the duty cycle is 300 s). The coherence losses also increase with the source’s angular separation, due to residual long term phase variations which distort the image. Nevertheless, neither of these quantities are sensitive to error processes that cause systematic position offsets, such as those expected from the spatial structure, direction dependent nature, of the ionospheric errors.

4) *Accuracy*: The observed quasars were selected from a VLBI catalog with precise positions with accuracies  $\sim 0.2$  mas (rfc\_2015b). Differences of no more than a few mas between the catalog positions and the relative astrometric measurements presented in this paper are expected, arising from the effects that effectively change the measured positions. These are: the use of group delays observable in geodetic analysis compared to the phase delays in our relative astrometry analysis (Porcas 2009), expected position changes in the observed core at different frequencies (i.e. the core-shift effect) and differential structure blending effects between the observing frequencies of the catalog (8.4 GHz) and our observations (1.6 GHz).

## 4. Results

The main goal of these observations was to demonstrate the feasibility of MV to achieve high precision astrometry at low frequencies, along with a comparative study between MV and PR.

### 4.1. Calibrated Visibility Phases and Astrometric Images: MV vs. PR

*Visibility Phases*: Fig. 2 shows a superposition of the residual relative visibility phases of C4 for a representative subset of baselines, after calibration using PR (analysis id: PR<sub>2°</sub>, PR<sub>4°</sub> and PR<sub>6°</sub>) and MV (analysis id: MV<sub>QSO</sub>) for the same range of target-calibrator angular separations, from epochs I (left) and II (right). The long time-scale trends in PR analysis are easily appreciated: the deviations from zero are increasingly large for pairs with larger angular separation and are different in the two epochs, with epoch II being significantly better. This is indicative of systematic residual phase errors, which depend on the weather conditions. Satellite-based Global Positioning System (GPS) data <sup>2</sup> are consistent with epoch II ionospheric conditions being more benign. The largest disturbances are seen at the beginning of the observations, which correspond to the sunrise. Note that, in epoch II, the phases for the 6° angular separation pair are larger (by about a factor of ca. 3) and with opposite sign compared to those for the 2° pair and that they correspond to calibrators on opposite sides of the target. This is consistent with the expectations from a wedge-like ionospheric structure responsible for direction dependent errors as described in Section 3.1.

---

<sup>2</sup>The GPS ionospheric data comes from the US Total Electron Content Product Archive of the National Oceanic and Atmospheric Administration (NOAA). <https://www.ngdc.noaa.gov/stp/IONO/USTEC/>

MV results in the smallest phase residuals (significantly smaller than  $PR_{2^\circ}$ ) with almost none of the signatures for sunrise or systematic trends visible in PR, and are similar for both epochs. All of these are indicative of a superior performance on the mitigation of ionospheric errors regardless of the weather conditions. This is crucial for accurate single- and multi-epoch astrometric analysis, as shown in the next section.

*Astrometric images:* The calibrated visibilities are used to generate the final product of the analysis, the astrometric images, which convey the astrometric measurements presented in the next section. Fig. 3 shows the MVed image for the C4 quasar obtained using the three calibrators together and the three PRed images using a single calibrator  $\sim 2^\circ$ ,  $4^\circ$  and  $6^\circ$  away, for the two epochs. The image degradation arises from remaining short and long term residual phase variations in each analysis. A qualitative comparison suggests that the PRed images improve with closer angular separations, as expected; that the MV is similar to  $PR_{2^\circ}$  at both epochs, with MV slightly better at epoch I, under worse weather conditions. Fig. 5 shows the self calibrated maps of the observed quasars. For a quantitative comparison, Table 4 lists the peak brightness and rms noise values in the astrometric images along with the coherence losses (i.e. FFR) estimated with respect to the self calibrated images, for the two epochs of observations. The corresponding astrometric thermal noise errors, estimated as described in section 3.2, are listed in Table 5. Nevertheless, as stated above, these estimates are not sensitive to residual systematic errors, which propagate into position shifts while maintaining the quality of the image. Those are better addressed by the repeatability errors, presented in the next section.

## 4.2. Astrometric Repeatability

Astrometry is performed directly in the images of quasar C4 shown in Fig. 3 by measuring the offset of the peak of brightness from the center of the map. This offset corresponds to the difference between our measurements and the catalog positions used for correlation. Fig. 4a shows the astrometric measurements, or offsets, of the target quasar C4 using PR (analysis id.  $PR_{2^\circ}$ ,  $PR_{4^\circ}$ ,  $PR_{6^\circ}$ ) and MV (analysis id.:  $MV_{QSO}$ ) at the two epochs of observations. Fig. 4b shows an expansion of the area around the MV measurements at the two epochs. The astrometric uncertainties in the plot are  $1-\sigma$  thermal noise error bars ( $\sigma_{pos,thermal}$ ) listed in Table 5.

Note that, in general, while the PR and MV measurements at a given epoch are expected to differ, because they are tied to different reference points, the inter-epoch differences convey information on the source position changes (if any) undergone in the 1-month time span between the two epochs. For stationary sources, as it is the case for quasars, no or negligible

position changes are expected. Therefore one can estimate the repeatability errors using the change in the measured offsets at the two epochs for a given technique. Table 5 lists the repeatability errors estimated as described in Section 3.2 which are an empirical estimate of the astrometric precision. It is immediately obvious that the repeatability errors are much larger for PR, compared to those for MV. Also, that the repeatability errors are larger than the thermal noise errors for PR; instead they are within the  $1\sigma$  thermal noise error bars for MV.

Fig. 4c displays the repeatability errors as a function of source pair angular separations, for PR analysis. This linear trend is as expected from PR analysis, as closer angular separations provide a better atmospheric compensation. The MV repeatability errors are the smallest, more than one order of magnitude smaller than those for the closest pair with PR, and are equivalent to those from a very close pair of sources (i.e. close to zero angular separation) in PR analysis. It is worth highlighting that instead the MV and PR<sub>2°</sub> images are of similar quality and have similar FFR values. This underlines the insensitivity of the PRed images to large systematic errors. This underlines the superior quality of the calibration of atmospheric errors using multiple calibrators, compared to that achieved with a single calibrator with the same range of angular separations, and that MV analysis leads to higher precision astrometry. This is in agreement with the findings from our previous simulation studies, where we concluded that using multiple calibrator sources with MV resulted in one order of magnitude improvement compared to PR with a single calibrator (Jimenez-Monferrer et al. 2010; Dodson et al. 2013).

Fig. 4a also conveys qualitative information on the astrometric accuracy of the different calibration techniques since the observed quasars have well determined positions in the rfc\_2015b catalog. We expect offsets of no more than a few (ca. 1-2) mas to account for differences between both measurements in all cases (see discussion in Section 3). Hence the magnitude of each of the astrometric offsets in Fig. 4a is indicative of the accuracy of that measurement and the method. PR offsets increase for larger source separations; MV results in the smallest offsets which indicates higher calibration accuracy. In fact, the magnitude of the accuracies is similar to the repeatability errors listed in Table 5.

Finally, the distribution of the measurements in Fig. 4a is also indicative of the spatial structure of the propagation medium being a planar surface. There is a resemblance between the geometric distribution of the three PR estimates at epoch I (i.e. PR<sub>2°</sub>.I, PR<sub>4°</sub>.I, PR<sub>6°</sub>.I) and epoch II (i.e. PR<sub>2°</sub>.II, PR<sub>4°</sub>.II, PR<sub>6°</sub>.II). Such distributions would arise from planar spatial structures in the propagation medium above each antenna, where the size and orientation of the triangles at each epoch depend on the weather conditions at a given epoch. The triangle for epoch I is more elongated than for epoch II. Moreover, both triangles appear rotated with respect to each other around a pivot point which is close to the MV measurements,

which remain practically unchanged (within the thermal noise error bars) at both epochs, regardless of the weather conditions, as is expected from a quality calibration.

### 4.3. Astrometry on OH-maser source: MV vs. in-beam PR

In this section we compare the astrometric results from PR with an “in-beam” calibrator and MV with more distant calibrators, based on the analysis using the spectral line OH-maser as the target source (analysis Ids:  $PR_{in-beam}$  and  $MV_{OH}$ , respectively, in Table 2). The  $PR_{in-beam}$  analysis uses the simultaneous observations of C4 and the OH maser target source,  $0.4^\circ$  away; the MV analysis uses the alternating observations between the target line source and the three (continuum) calibrators C1, C2 and C3, which are  $\sim 2^\circ$ ,  $4^\circ$ , and  $6^\circ$  away. Fig. 6a shows the astrometric offsets estimated at epoch II, with respect to epoch I, for both analyses. This accounts for the different reference points in PR and MV and permits a direct comparison of the inter-epoch differences. The estimated thermal noise errors are  $\sigma_{pos,thermal} \sim \pm 0.5$  mas and  $\sim \pm 1$  mas in right ascension and declination, respectively. Note that, in this case, the inter-epoch differences trace the expected motion of the stellar target, due to the proper motion and parallax, during the 1 month interval between epochs. Hence, unlike the case of quasar-only analysis described in the section above, the astrometric changes between the two epochs are not a direct measure of the repeatability errors (and the precision of the method) and an extra step is required to eliminate the contribution from the motion of the source.

We used a set of four in-beam phase referencing observations spanning 1 year to measure the proper motion and parallax of the OH maser target source (Orosz et al. 2016). These include the two epochs described in this paper, plus two additional epochs with a similar observing configuration, except for having longer duty cycle times ( $\sim 10$  minutes) which prevented MV analysis. The measured parallax is  $\pi = 2.74 \pm 0.39$  mas and the proper motion is  $\mu(\alpha, \delta) = (-0.17 \pm 0.8 \text{ mas yr}^{-1}, -7.64 \pm 0.80 \text{ mas yr}^{-1})$ . Fig. 6b is same as Fig. 6a, after removing the contributions from the proper motion and parallax between epochs I and II, with the repeatability errors being  $\sigma_{pos,rep}^{MV_{OH}} = 0.29$  mas for  $MV_{OH}$  and  $\sigma_{pos,rep}^{PR_{in-beam}} = 0.62$  mas for  $PR_{in-beam}$ . The repeatability errors for  $MV_{OH}$  are half the magnitude for  $PR_{in-beam}$ , albeit based on more distant calibrators. In this case all measurements agree within the thermal noise errors, which are larger for the case of a weak source.

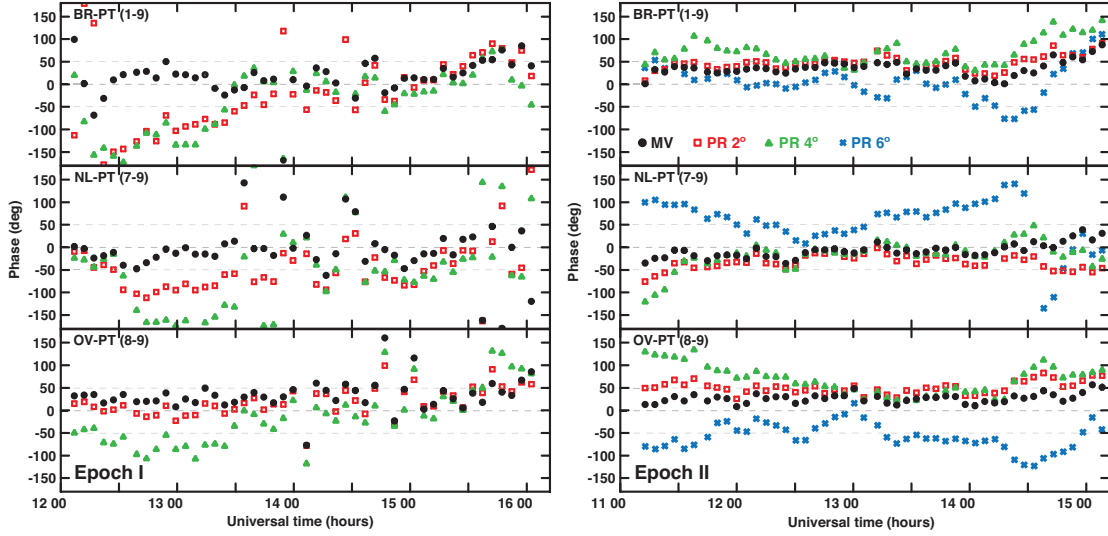


Fig. 2.— Calibrated visibility phases for C4 using MV (black dots) with three calibrators, and PR with a calibrator  $2^\circ$  (red squares),  $4^\circ$  (green triangles) and  $6^\circ$  (blue crosses, Epoch II only) away, on a subgroup of baselines, in Epoch I (left) and Epoch II (right).

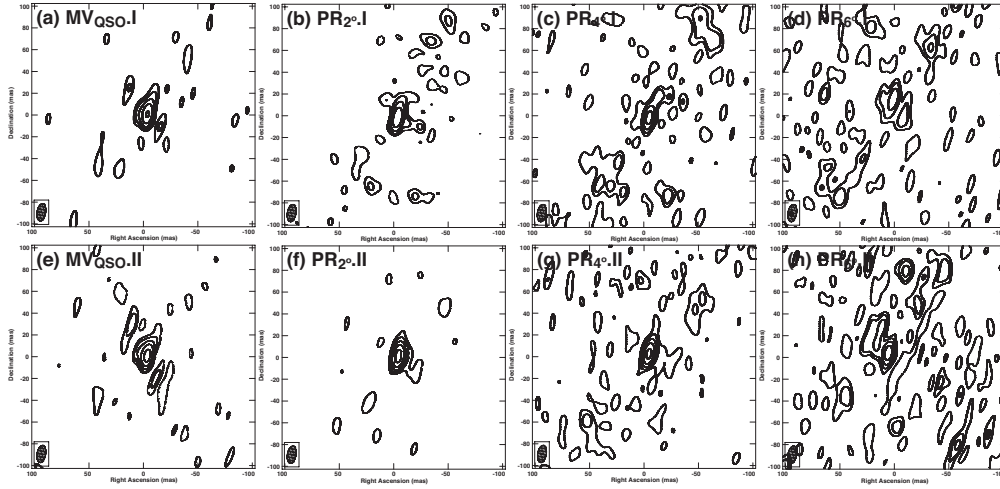


Fig. 3.— Astrometric images of C4 using analyses compared in this paper. From left to right, MV,  $PR_{2^\circ}$ ,  $PR_{4^\circ}$  and  $PR_{6^\circ}$ , for epoch I (upper row) and epoch II (lower row). The lowest intensity contour in all images are at  $3\text{-}\sigma$  level of the MV map and doubling thereafter. The images have been restored with the same beam:  $8 \times 16$  mas with  $PA = -10^\circ$ . See Table 4 for values of peak brightness, rms noise and astrometric offsets in the images.

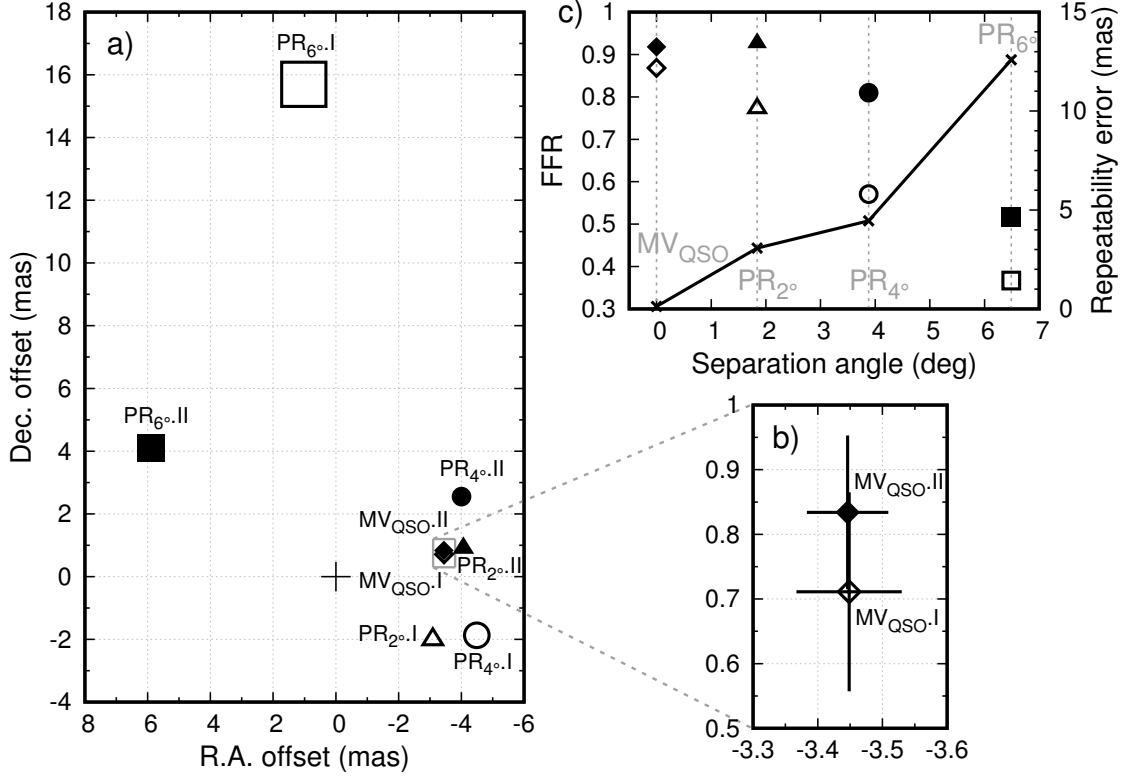


Fig. 4.— *a)* Astrometric offsets in the angular separations measured with MV, PR<sub>2°</sub>, PR<sub>4°</sub> and PR<sub>6°</sub> analyses (see Table 2 for description), from the observations of quasars at the two epochs, with respect to those in the VLBA radio fundamental catalog rfc\_2015b. The size of the plotted symbols corresponds to the estimated thermal noise error in each case (see Table 5). The labels describe the analysis id. and epoch of observations. *b)* Zoom for MV astrometric solutions. The error bars are the thermal noise errors. Both epochs agree within the error bars. *c)* Solid line shows the corresponding repeatability astrometric errors versus the angular separation between target and calibrator for PR analysis, and for an effective 0° separation for MV. Filled and empty symbols show the Flux Fractional Recovery quantity versus angular separation for MV (diamond), PR<sub>2°</sub> (triangle), PR<sub>4°</sub> (circle), and PR<sub>6°</sub> (square) analyses, for epoch I (empty) and epoch II (filled).

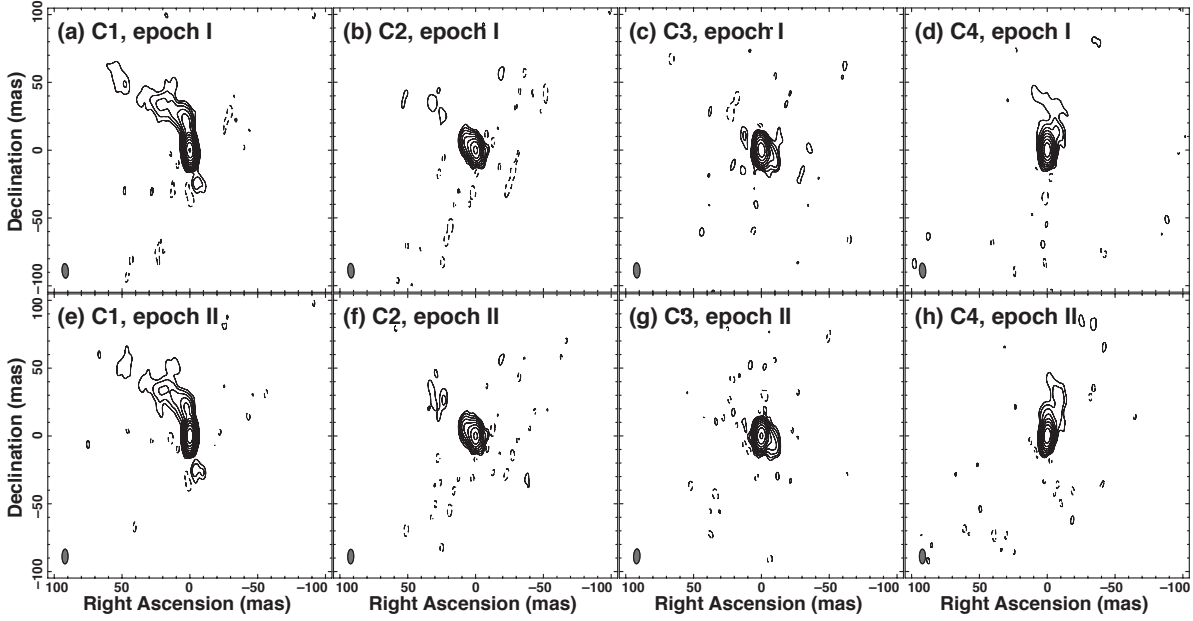


Fig. 5.— Self-calibrated maps of the observed quasars. The peak brightness are listed in Table 1. The lowest intensity contour is the  $3\text{-}\sigma$  level and doubling thereafter. Restoring beam is  $8 \times 16$  mas with  $\text{PA} = -10^\circ$ .

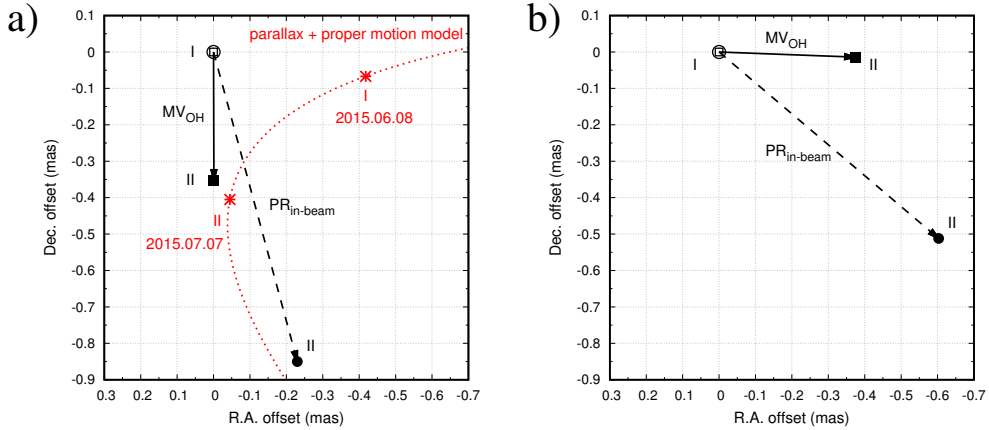


Fig. 6.— *a*) Astrometric changes in the position of the line source OH measured with MV and  $\text{PR}_{in-beam}$  at epoch II, with respect to epoch I. The estimated thermal noise errors are 0.5 mas and are not displayed. The labels describe the analysis id. and epoch of observations. Also shown is the expected apparent motion of the OH-maser source between both epochs, due to the proper motion and parallax (see text). *b*) Same as *left*, after correcting for the apparent motion of OH-maser source due to the proper motion and parallax.



Epoch	Analysis Id.	Sep. (deg)	Peak (mJy/beam)	rms (mJy/beam)	FFR (%)	Astrometric Offset	
						$\Delta_{RA}$ (mas)	$\Delta_{DEC}$ (mas)
I	MV <sub>QSO</sub>	$\sim 0.$	64	1	87	-3.45	0.71
I	PR <sub>2°</sub>	1.8	57	1	77	-3.09	-2.02
I	PR <sub>4°</sub>	3.9	42	2	57	-4.49	-1.87
I	PR <sub>6°</sub>	6.5	27	2	37	1.02	15.70
II	MV <sub>QSO</sub>	$\sim 0.$	67	1	92	-3.45	0.83
II	PR <sub>2°</sub>	1.8	67	1	93	-4.06	0.90
II	PR <sub>4°</sub>	3.9	59	1	81	-4.01	2.55
II	PR <sub>6°</sub>	6.5	38	2	52	5.89	4.09

Table 4: Outcomes from astrometric analyses. Column 1 is the epoch of observations. Columns 2 and 3 are the analysis id. and source angular separation, respectively. Columns 4, 5 and 6 are the peak brightness, rms noise and Fractional Flux Recovery values measured from the astrometric images in Fig. 3, respectively. Columns 7 and 8 are the astrometric offsets of the peak of brightness in the astrometric images shown in Fig. 3 from the centre of the map; these are shown in Fig. 4a).

## 5. Discussion and Conclusions

### *Demonstration of MultiView high precision astrometry at low frequencies*

The ionospheric propagation effects are the main limitation to routinely achieving high precision astrometry at frequencies *ca.*  $< 8$  GHz, using state-of-the-art phase referencing methods developed for higher frequencies. This is due to the distinct direction dependent signature, which limits high precision measurements to cases when there is a suitable very close calibrator *ca.* arcmins away. Our combination of multiple calibrators around the target results in a significant reduction of the systematic astrometric errors, from the mitigation of the spatial structure effects, by using a 2-D linear (spatial) interpolation to estimate the calibration along the direction of the target source.

We have presented an empirical demonstration of the superior mitigation of MV along with a comparative study with phase referencing analysis using a single source at a range of angular separations, including “in-beam” phase referencing. All the analysis have been carried out using the same VLBA observations at 1.6 GHz. We have used the repeatability between two epochs of observations to provide an empirical estimate of the systematic astrometric errors, which are otherwise very difficult to quantify.

We achieve high precision MV astrometry of *ca.*  $100 \mu\text{as}$  in a single epoch of observations of quasars with calibrators at  $2^\circ$  and larger angular separations, effectively reaching the thermal noise limit of the observations. This corresponds to more than an order of magnitude

Analysis Id.	$\sigma_{pos,thermal}$ (mas)		$\sigma_{pos,rep}$ (mas)
	Epoch I	Epoch II	$\Delta'_{I-II}$
MV <sub>QSO</sub>	0.17	0.14	0.1
PR <sub>2°</sub>	0.19	0.11	2.7
PR <sub>4°</sub>	0.42	0.22	3.9
PR <sub>6°</sub>	0.75	0.44	11.2

Table 5: Empirically estimated astrometric errors for measurements presented in this paper. Column 1 is the calibration strategy (see Table 2 for description). Columns 2 and 3 are the thermal noise errors for epochs I and II, respectively. They have been calculated using the values listed in Table 4 with a beam of  $8 \times 16$  mas PA= $-10^\circ$ . Column 4 lists the repeatability errors, calculated from the astrometric offsets in Table 4 and corrected for bias for two epochs, with  $\Delta'_{I-II} = \Delta_{I-II} / \sqrt{2} * \sqrt{2/\pi}$ . See Section 3.2 for description of error analysis.

improvement with respect to the precision achieved using PR with a single calibrator  $2^\circ$  away, which is ca. 3 mas, due to the residual systematic errors in the analysis. This underlines the importance of correcting for the spatial structure of the ionospheric residuals. The comparative improvement can be interpreted as MV compensation being equivalent to that from PR with a single calibrator ca. 10 times closer, in this case ca.  $0.2^\circ$  away, assuming a linear dependence between astrometric precision and target–calibrator angular separation. Also, our results indicate that there is a common limiting factor for accuracy and precision, namely the residual ionospheric propagation errors, and both are improved by a quality calibration as provided by MV.

We have also demonstrated the performance in the weak source case using the observations of the OH-maser line source, and compared MV using  $2^\circ$ ,  $4^\circ$  and  $6^\circ$  angular separations with ‘in beam’ PR using a calibrator  $0.4^\circ$  away. The repeatability errors are larger, as expected from lower SNR, but interestingly keep the same corresponding relative astrometric signature found in the analysis of the quasars. That is MV<sub>OH</sub> calibration is a factor of two better, with respect to PR<sub>in-beam</sub> using a calibrator five times closer to the target. Therefore we have demonstrated the benefits of using multiple calibrators, in our case with an improvement of more than one order of magnitude in astrometric precision, reaching the thermal limit of the observations, of  $\sim 100\mu\text{as}$ . In general we expect MV to be relevant for observations in the frequency regime where the ionospheric effects continue to be the dominant source of errors, that is, in observations up to ca. 8 GHz. We conclude that greater improvements are expected from increased sensitivity, and faster duty cycles, with maximum benefits from simultaneous observations and closer source distribution, to minimize the non-linear deviations of the actual ionospheric spatial structure above each antenna

from a planar surface.

*MV in the context of SKA and multi-beam instruments*

Precise astrometric capability is of great importance in the SKA era. It is a SKA goal to achieve  $10\ \mu\text{as}$  astrometric accuracy at a single epoch of observations at  $\sim 1.4\ \text{GHz}$  (Paragi et al. 2014). The high sensitivity and long baselines of SKA VLBI observations will result in a much reduced thermal noise level and high spatial resolution. Therefore this goal is achievable as long as a sufficiently accurate ionospheric phase calibration strategy is in place. For a single calibrator source and PR techniques, the required angular separation to the target would be ca. 1 arcmin (Paragi et al. 2014). This puts a very tight limit on the number of available calibrator sources, even at the SKA sensitivities (Godfrey et al. 2011). This constraint on the angular separation can be significantly relaxed, by using multiple calibrator sources and MV techniques, as suggested by the demonstration presented in this paper and our previous simulation studies. Additionally, the multi-beam capability of SKA will allow for simultaneous observations of all sources and therefore eliminate the errors arising from short term phase fluctuations, which result in a reduction of the coherence losses (i.e. characterized by FFR quantity) and the thermal noise errors, while improving the overall performance. This applies to other instruments with multibeam systems such as ASKAP and Westerbork Synthesis Radio Telescope with Apertif, among others. Our demonstration includes three calibrators; note that the more calibrators the better, as this will allow the most accurate reconstruction of the atmospheric effects. Therefore we expect MV can deliver the goal of  $10\ \mu\text{as}$  astrometry for many targets with SKA.

*Other relevant scientific applications of MV*

Next we consider other scientific applications.

**Near Field Cosmology:** This paper used astrometric observations of a group of quasars in the role of targets and calibrators and an OH maser source in the ground state at 1.6 GHz. Scientific applications using such a group of sources applied to studies with the SKA of the nearby universe, including the Milky Way galaxy and the Local Group of galaxies are described in Imai et al. (2016). Although that case-study report discussed the scientific applications conservatively based on only ‘in-beam’ PR astrometry, our results indicate that MV would provide further benefits.

**Pulsars at 1.6 GHz:** Our empirically estimated MV astrometric accuracy of ca.  $100\ \mu\text{as}$  at 1.6 GHz with VLBA observations, using calibrators more than ca.  $2^\circ$  away is at the state-of-the-art, only comparable with ‘in-beam’ phase referencing observations with a calibrator ca. 10s of arcminutes away (Deller et al. 2013, 2016). This improvement is expected to

continue to apply at all angular scales. Hence, using three calibrators within the SKA-Mid antenna beams and MV will result in a further increase by one order of magnitude of the astrometric precision, extrapolating from our comparative study. In general, allowing for larger angular separations makes it possible to select good calibrator sources, which are fundamental for multi-epoch studies. With the higher probabilities of finding suitable calibrators the general applicability is also highly increased. In some cases, such as pulsar observations in the galactic plane, it might even be desirable to use calibrators out of the plane to reduce the effect of scattering. This would be possible using MV.

**Methanol masers at 6.7 GHz:** High precision astrometry observations of methanol masers at 6.7 GHz holds the prospect to contribute to the successful program for 3-D mapping of our Galaxy, as a complement to the precise water maser measurements (Reid et al. 2014). However the advanced PR strategies used at 22 GHz, in the tropospheric dominated regime, fail to provide high precision astrometry at 6.7 GHz, as this is in the ionospheric dominated regime. Therefore MV with fast source switching between sources, or simultaneous observations if possible, provides a strategy for superior calibration of the tropospheric and ionospheric errors resulting in precise astrometry.

#### **Acknowledgements**

The VLBA is operated by National Radio Astronomy Observatory and is a facility of the National Science Foundation operated under cooperative agreement with Associated Universities Inc.. GO and HI have been supported by the JSPS Bilateral Collaboration Program and KAKENHI programs 25610043 and 16H02167. MR, RD, GO and HI acknowledge support from DFAT grant AJF-124. This research has made use of the SIMBAD database, operated at CDS, Strasbourg, France.

#### **REFERENCES**

- Alef, W. 1988, in IAU Symposium, Vol. 129, The Impact of VLBI on Astrophysics and Geophysics, ed. M. J. Reid & J. M. Moran, 523
- Deller, A. T., Boyles, J., Lorimer, D. R., et al. 2013, *ApJ*, 770, 145
- Deller, A. T., Vigeland, S. J., Kaplan, D. L., et al. 2016, *ApJ*, 828, 8
- Dodson, R., Rioja, M., Asaki, Y., et al. 2013, *AJ*, 145, 147
- Dodson, R., Rioja, M., Molina, S., & Gómez, J. 2016, Submitted

- Doi, A., Fujisawa, K., Habe, A., et al. 2006, PASJ, 58, 777
- Fomalont, E. B., Goss, W. M., Beasley, A. J., & Chatterjee, S. 1999, AJ, 117, 3025
- Fomalont, E. B., & Kopeikin, S. 2002, in Proceedings of the 6th EVN Symposium, ed. E. Ros, R. W. Porcas, A. P. Lobanov, & J. A. Zensus, 53
- Godfrey, L., Bignall, H., & Tingay, S. 2011, Very High Angular Resolution Science with the SKA, Tech. rep., Curtin University, Australia
- Greisen, E. W. 2003, Information Handling in Astronomy - Historical Vistas, 285, 109
- Honma, M., Tamura, Y., & Reid, M. J. 2008, PASJ, 60, 951
- Imai, H., Burns, R. A., Yamada, Y., et al. 2016, ArXiv e-prints
- Jimenez-Monferrer, S., Rioja, M. J., Dodson, R., Smirnov, O., & Guirado, J. C. 2010, in 10th European VLBI Network Symposium and EVN Users Meeting: VLBI and the New Generation of Radio Arrays, Manchester, Proceedings of Science, Vol. 125, 84
- Orosz, G., Imai, H., Dodson, R., et al. 2016, Submitted
- Paragi, Z., Godfrey, L., Reynolds, C., et al. 2014, ArXiv e-prints
- Porcas, R. W. 2009, A&A, 505, L1
- Porcas, R. W., & Rioja, M. J. 2002, in Proceedings of the 6th EVN Symposium, ed. E. Ros, R. W. Porcas, A. P. Lobanov, & J. A. Zensus, 65
- Reid, M. J., & Brunthaler, A. 2004, ApJ, 616, 872
- Reid, M. J., & Honma, M. 2014, ARAA, 52, 339
- Reid, M. J., Menten, K. M., Brunthaler, A., et al. 2014, ApJ, 783, 130
- Rioja, M., & Dodson, R. 2011, AJ, 141, 114
- Rioja, M., Dodson, R., Porcas, R. W., et al. 2009, in 8th International e-VLBI Workshop, 14
- Rioja, M. J., Porcas, R. W., Desmurs, J.-F., et al. 2002, in Proceedings of the 6th EVN Symposium, ed. E. Ros, R. W. Porcas, A. P. Lobanov, & J. A. Zensus, 57
- Rioja, M. J., Stevens, E., Gurvits, L., et al. 1997, Vistas in Astronomy, 41, 213

Shepherd, M. C., Pearson, T. J., & Taylor, G. B. 1994, in Bulletin of the American Astronomical Society, Vol. 26, Bulletin of the American Astronomical Society, 987–989

Wrobel, J., Walker, R., Benson, J., & A., B. 2000, VLBA Scientific Memorandum n. 24: Strategies for Phase Referencing with the VLBA, Tech. rep., NRAO